Sains Malaysiana 53(11)(2024): 3555-3571
http://doi.org/10.17576/jsm-2024-5311-02

Integrating Petrography and Geochemistry Data for Provenance and Palaeotectonic Interpretation of a Sedimentary Deposit

(Mengintegrasikan Data Petrografi dan Geokimia untuk Tafsiran Asal dan Palaeotektonik bagi Deposit Sedimen)

SALUFU EMMANUEL OMOH, HABIBAH JAMIL* & NORASIAH SULAIMAN

Department of Earth Sciences and Environment, Faculty of Science and Technology, Universiti Kebangsaan Malaysia, 43600 UKM Bangi, Selangor, Malaysia

Received: 29 December 2023/Accepted: 3 October 2024

ABSTRACT

Effective interpretation of provenance and tectonic settings that affected a sedimentary deposit was optimised using a geochemistry and mineralogical interdisciplinary approach. Geochemical data was integrated with petrographic data to interpret the provenance and tectonic history of some sedimentary samples selected from a sedimentary sequence exposed along Imiegba in southern Nigeria. Sixteen samples were subjected to X-ray Fluorescence (XRF) analysis to assess the essential oxide composition and eighteen were analysed for their rare earth element compositions. Ten sedimentary samples were prepared into thin sections for a mineralogical study under a petrographic microscope. The geochemical approach using the compositional plot of TiO_2, Al_2O_3, Fe_2O_3, MgO, CaO, Na_2O and K_2O of the samples on a discriminant function shows a Felsic igneous source which is confirmed by the enrichment in the light rare earth elements concentration. It also indicates intermediate and Quartzose sedimentary provenance on a passive margin and oceanic island arc. The modal composition of quartz, feldspar and rock fragments plotted on a triangular diagram indicate metamorphic, plutonic and recycled orogen provenances, with a cratonic interior, and continent transitional and basement uplift activities. The study area thus contains sedimentary deposits derived from plutonic, metamorphic, and quartzose sedimentary provenance with imprints of divergent tectonic and convergent tectonic activities.

Keywords: Geochemistry; palaeotectonic; petrography; provenance; sedimentary

ABSTRAK

Tafsiran berkesan bagi tetapan asal dan tektonik yang menjejaskan mendapan sedimen telah dioptimumkan menggunakan pendekatan antara disiplin geokimia dan mineralogi. Data geokimia telah disepadukan dengan data petrografi untuk mentafsirkan sejarah asal dan tektonik beberapa sampel sedimen yang dipilih daripada jujukan sedimen yang terdedah di sepanjang Imiegba di selatan Nigeria. Enam belas sampel telah tertakluk kepada analisis pendarfluor sinar-x (XRF) untuk menilai komposisi oksida penting manakala lapan belas telah dianalisis untuk komposisi unsur nadir bumi mereka. Sepuluh sampel sedimen telah disediakan ke dalam bahagian nipis untuk kajian mineralogi di bawah mikroskop petrografi. Pendekatan geokimia menggunakan plot komposisi sampel TiO_2, Al_2O_3, Fe_2O_3, MgO, CaO, Na_2O dan K_2O pada fungsi diskriminasi menunjukkan sumber igneus Felsik yang disahkan oleh pengayaan dalam kepekatan unsur nadir bumi ringan. Ia juga menunjukkan asal sedimen perantaraan dan Kuartzos pada margin pasif dan arka pulau lautan. Komposisi modal serpihan kuarza, feldspar dan batuan yang diplotkan pada rajah segi tiga menunjukkan asal-usul orogen metamorfik, plutonik dan kitar semula dengan bahagian dalam kratonik dan benua aktiviti peralihan dan tingkatan bawah tanah. Kawasan kajian itu mengandungi mendapan sedimen yang diperoleh daripada asal enapan plutonik, metamorfik dan kuarzos dengan kesan aktiviti tektonik tektonik dan tektonik bercapah.

Kata kunci: Asal; geokimia; paleotektonik; petrografi; sedimen

INTRODUCTION

The source area's weathering history, provenance, and tectonics of sedimentary deposits are essential for detailed basin evaluation and hydrocarbon exploration. Several authors have used different methods to determine sedimentary deposits' provenance and tectonic evolution. Overare et al. (2020) used the geochemical composition of the sedimentary sequence in the south-eastern Anambra

basin to deduce provenance and tectonic settings. Tijani, Nton and Kitagawa (2010) deduced the provenance of the south-eastern Anambra basin using geochemical and granulometry approaches. Madukwe and Obasi (2015) used geochemistry to delineate the provenance and tectonic settings of the Ogwashi-asaba formation in the Anambra basin. Ogala et al. (2015) used petrography methods to assess provenance and tectonics evolution. However, this study combines the petrography and geochemistry data (X-ray fluorescence, XRF) to optimise the interpretation of a sedimentary deposit's provenance and tectonic settings in the study area (western arm of the Anambra Basin).

Sedimentary samples were selected from the Manu formation section in the Imiegba area within the western Anambra basin in southwest Nigeria for petrography study and geochemistry analysis. The area was chosen as a case study because not much work has been done on the tectonic history and provenance of the western Anambra basin compared to the eastern Anambra basin where several works on tectonic events and provenance have been conducted. Similarly, the nature of the basin also gives us the privilege of comparing our results with the results of researchers who have worked in the eastern Anambra basin. Anambra basin was formed during the breaking of the Gondwana supercontinent and it covers an area of 55, 000 km^2 bounded by the Benin Hinge in the west and Benue Trough in the east and the Niger Delta in the south (Edegbai, Schwark & Oboh-Ikuenobe 2020).

GEOLOGICAL SETTINGS

The study area is located within the western Anambra Basin, Southern Nigeria (Figure 1). The Anambra Basin is essentially known to be one of the Nigerian Basins that conserves commercial deposits of coal (Nwanjide 2013; Okoro, Igwe & Nwajide 2016). The Basin stretches from Southeast Nigeria where it was first discovered and extends through Southwest to Northern Central. The Basin exposure in the Southeast has been studied extensively. The stratigraphy sequence of the Basin includes the Nkporo and Enugu Formations which contain the Campanian sedimentary deposit (Nwanjide 2013). The Mamu Formation contains late Campanian to mid-Maastrichtian sediment, and the Ajali Formation comprises mid-Maastrichtian sediments. The Nsukka Formation contains a mid to late Maastrichtian deposit, the Imo group contains a Paleocene deposit of shale and the Ameki and Nanka Formation contain an Eocene sedimentary sequence of sandstone (Nwanjide 2013). The basin holds the Campanian to the Eocene siliciclastic sedimentary deposits (Adeigbe & Salufu 2009; Nwanjide 2013). The tectonic evolution of the Anambra basin was linked to the aborted rifted valley system described as aulacogen in the lower Benue trough (Obaje 2019). This tectonic evolution accompanied the separation of the African and South American plates and it represents the third cycle in the evolution of the trough and its associated basin (Ameh 2019). Representative samples were selected from the Mamu formation within the basin for the study area (Figure 1(a)). The lithofacies in the study area comprise sandstone, coal, shales, siltstone, mudstones, and Kaolin deposits.

MATERIALS AND METHODS

A total of forty-four samples were used for the research: Ten sandstone samples were subjected to petrographic analysis, sixteen sedimentary samples were subjected to X-ray Fluorescence (XRF) analysis and eighteen sedimentary samples were subjected to Induce Coupled Plasma-Mass Spectroscopy (ICP-MS) analysis. Based on the lithological composition and the stratigraphy sequence's thickness, thirty-four samples comprising shales (two samples), coal (one sample), and mudstone (one sample) and the rest sandstone samples were prepared for XRF and ICP-MS. The samples were oven-dried at 80 °C and ground into powder by an iron steel ball mill at the Department of Earth Sciences and Environment, Universiti Kebangsaan Malaysia. Eighteen samples were digested for ICP-MS from the pulverized samples. 0.5 g of the inorganic siliciclastic pulverized rock samples (or 0.25 g of organic pulverized rock) were measured into different Teflon containers. For the Teflon with the pulverized inorganic rock sample, 9 mils of Nitric acid, 3 mils of Hydrogen fluoride, 2 mils of Hydrogen chloride, and 1 mils of water were added to the Teflon containing the inorganic samples. For the organic sample, 9 mils of Nitric acid, followed by 3 mL of hydrogen chloride, 2 mils of hydrogen peroxide (effervescence occur and allowed to cool down) and 1 mil of water was added. The Teflon was corked and transferred to a microwave device for digestion. The mixture was heated in the microwave for 10 min to a temperature of 200 °C. The temperature was held at 200 °C for 20 min, and then the temperature was allowed to cool for 15 min. The mixture was removed from the microwave and the volume was made to 50 mils by adding ionized water. The solution was thereafter subjected to an inductively coupled plasma-mass spectrometry (ICP-MS) analysis to determine the composition of rare earth elements. Similarly, 5 g of the pulverized sixteen sedimentary rock samples were subjected to X-ray fluorescence (XRF) analysis, at the general laboratory facility at Universiti Kebangsaan Malaysia to estimate the composition of the major oxides in the samples using a procedure similar to that of James et al. (2021) and Rollinson (1993). Furthermore, sixteen sandstone samples

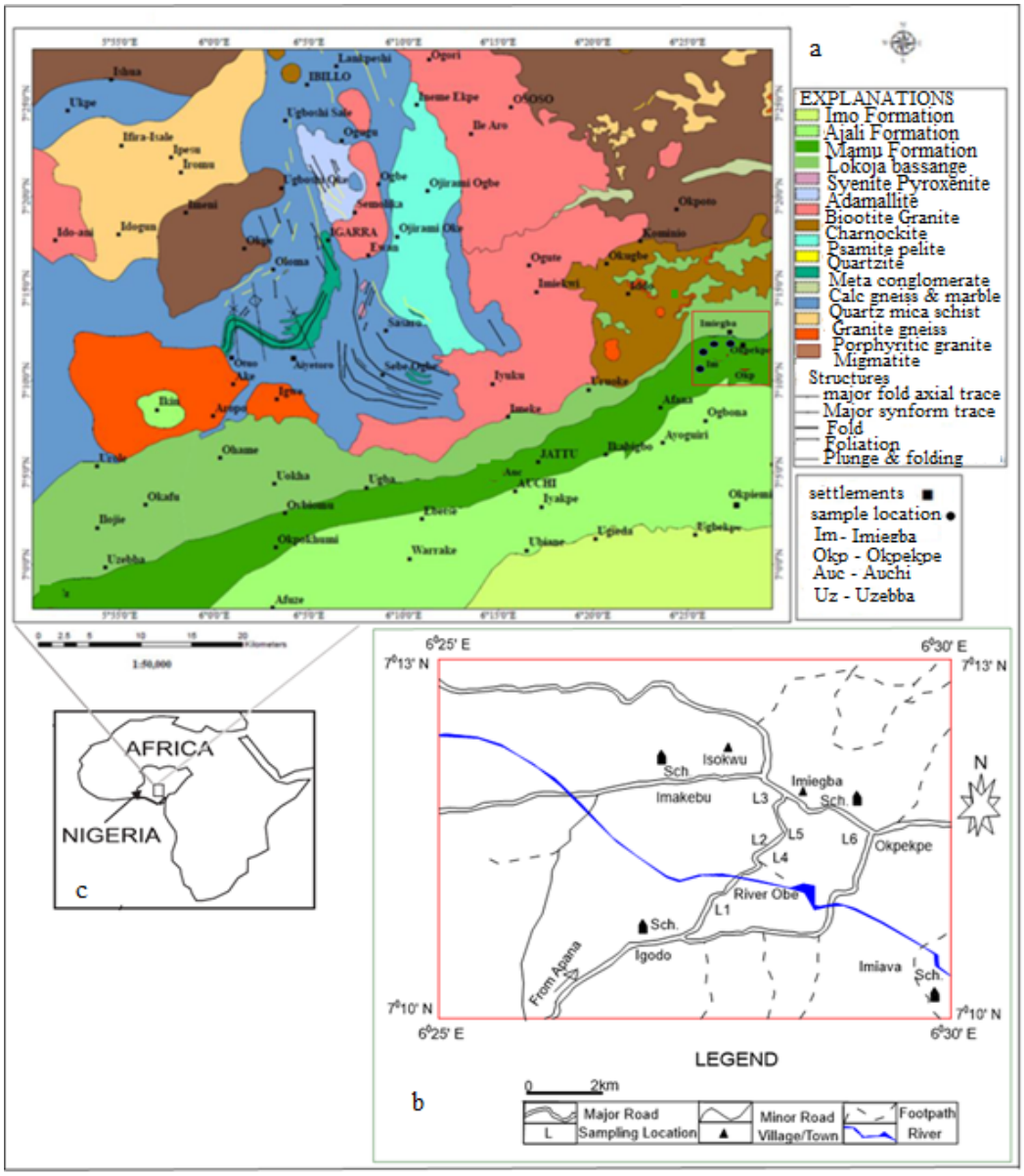

FIGURE 1. Chart showing the geologic map of the study area (a) and the study area's (b) location map (Modified after Nigerian Geological Survey Agency (NGSA) 2006)

were prepared into thin section specimens for petrography study using a method similar to Körmös et al. (2020). The mineralogical composition of the sandstone samples was determined by examining the thin sections and calculating the modal composition of Quartz=Q, Feldspar=F and Rock Fragment=RF under a petrographic microscope using a method similar to Mackenzie and Adams (2003) and Pettijohn, Potter and Silver (1987). The number of polycrystalline quartz=QP and monocrystalline quartz=Qm was estimated using a petrographic microscope. The sum of the QP and Qm comprises the total quartz composition in each thin section (Table 5). The percentage composition of Feldspar=F, Rock fragment=Rf and quartz=Q were plotted on a triangular diagram. The plot was used to infer the sedimentary deposit's provenance and palaeotectonic evolution.

The microwave digestion, ICP-MS was conducted at the geochemistry laboratory facility of the Faculty of Sciences and Technology, at Universiti Kebangsaan Malaysia. The cutting of the rock samples into thin-section specimens

and mineralogical microscopic analysis was done at the Department of Geology, University of Ibadan Nigeria and the Department of Earth Sciences and Environment, Universiti Kebangsaan Malaysia, respectively.

Before the geochemical results were adopted and used to interpret the provenance and palaeotectonic method of the deposit in the study area, the validity of the results (that is, the geochemical data) was cross-checked using the Pearson coefficient of correlation in the Statistical Package for the Social Sciences (SPSS). The sedimentary deposit's geochemical composition (REE and major element oxides) was used to delineate the provenance and palaeotectonic of the sedimentary deposit. This is because the geochemistry of a sedimentary rock is essential in interpreting the geological processes such as provenance, and palaeotectonic that have affected the sedimentary deposit (Rollinson 1993). Rare earth elements neither remobilise nor wash away during weathering or hydrothermal fluid (Rollinson 1993). Almost the exact composition of the Rare Earth Element (RRE) in the source rock is transferred or moved into the daughter rock. Hence, certain REE and major element oxides can be used to deduce the provenance, weathering and palaeotectonic due to their ability to withstand dissolution by weathering and transportation process.

RESULTS AND DISCUSSION

LITHOLOGICAL DESCRIPTION

A medium-grained 4.9 m thick sandstone underlies the sedimentary sequence. The sandstone is described as quartz arenite based on the composition of quartz (over 96%), feldspar, and lithic under aided eyes in the field. A 1.2 m grey-black coal overlies the sandstone unit. The third bed is indurated fine to medium-grained sandstone. The sandstone is 4.0 m thick and is described as quartz arenite due to its composition of over 95% quartz grains to feldspar and lithic when examined with an aided eye on the field. The fourth bed is a deposit of greyish-white Kaolin. It is 2.0 m thick, medium to coarse-grained with iron stain characteristics. The deposit contains a 25% composition of quartz similar to Arkosese (supplementary figure for the lithofacies log). The fifth bed is a deposit of 1.1 m greyish-black coal. The sixth bed is a deposit of greyish-brown siltstone (also described as a mudstone on the field) with burrows of Planolites and Thalassinoides (Figure 2(a)). The seventh bed is a 3.0 m grey-dark shale with a fissile characteristic. The rock comprises extra-formational clast and bivalve (Figure 2(b)). The eight-bed is a deposit of laminated siltstone. It is 6.0 m thick with fine grains. The ninth bed is a deposit of grey-black coal 0.3 m thick. The tenth bed is a deposit of organic siltstone. It is 3.0 m thick with organic matter. The eleventh bed is a heterolith which comprises an alternation of shale and siltstone. It is 8.0 m thick with a bivalve composition. This is overlain on top by a deposit of ferroginized sandstone described as quartz wacke 3.0 m thick and poorly sorted. The rock comprises fine grains of quartz of over 16% within larger quartz grains. The thirteenth bed is a deposit of sandstone referred to on the field as sub-litharenite since it contains less than 25% lithic composition. The rock is grey-white and 8.0 m thick. The rock is overlain on top by a ferroginized sandstone described as Arkosic arenite due to its composition of over 25% feldspar. The rock is friable and laminated with coarsening-up grain characteristics. It is 8.0 m thick. The fifteenth bed contains a deposit of sandstone with over 95% quartz grains. It is described as quartz arenite. The sixteenth bed is a 3.0 m thick white-grey siltstone. This is overlain by a sandstone with over 79% quartz composition. It is described as quartz arenite with 5.0 m thick and a coarsening up characteristic.

SEDIMENTARY GEOCHEMISTRY

The results of the X-ray fluorescence (XRF) and Induced coupled plasma-mass spectrometer (ICP-MS) analyses of the sedimentary samples from the study area are displayed in Tables 1 and 2, respectively. The concentrations of the essential oxides MgO (0.0141 - 0.514 wt %), CaO (0.0097 - 0.116 wt %), N_2O and K_2O in the analysed samples are all depleted (Table 1). However, the result shows enrichment in the concentration of SiO_2 (51.9-435 wt %) in all the samples. The concentration of Fe_2O_3 is also depleted except for samples s24 (3060 wt %), s33 (3300 wt %), s5 (9460 wt %), s11 (6160 wt %) and S14 (9430 wt %) which indicate high concentrations. The concentration of MnO and most of the samples' Na_2O are below the detection limit (BDL) (Table 1). The analysed samples' rare earth element compositions show enrichment in the light rare earth element (LREE) concentration over the Heavy rare earth elements (HREE) (Table 2).

From the correlation tables, Tables 3 and 4, respectively, the coefficient of correlation r = 0.502 – 0.802 for the major oxide and 510 – 991 for the REE; at 0.01 and 0.05 significance levels. It can be observed that there is a high positive significant correlation and a good positive linear relationship among the essential oxides and REE. This confirms the validity of the geochemical data and certifies the quality of the representative samples.

FIGURE 2. A bioturbated bed showing the imprint of Thalassanoides (horizontal branching burrow) and Planolites (vertical branching burrow) (a). A grey-black fissile shale with bivalve composition, (b). A poorly sorted laminated ferroginized quartz arenite (c), and An indurated quartz arenite (d)

PETROGRAPHY

The petrography results are presented in Figure 3 and Table 5. The percentage of polycrystalline and monocrystalline in the rock samples ranges from 50 to 86% and 5 to 26%, respectively, with some point and line grain contact. Sample s1 is medium to coarse-grained. It is poorly sorted with 98% quartz composition. The quartz crystals in the rock sample exhibit undulose extinction at 90º rotation. The quartz (98%), Feldspar (0%) and Lithic (2%) composition of the rock sample s01 falls in the Quartz arenite field when plotted on the Quartz (Q), Feldspar (F) and lithic (L) ternary diagram for rock classification. The rock sample s8 comprises 50% polycrystalline quartz, 15% monocrystalline quartz, 65% quartz and 35% feldspar (microcline) composition (Table 5(a)). No rock fragments were observed in the sample composition. When plotted on a ternary functional diagram for rock classification, the rock sample exhibited the characteristics of an Arkosic arenite (arkose), (Figure 3(a)). The rock sample s11 has a 77% feldspar and 23% quartz composition. The quartz crystals are fine to coarse grains with undulose extinction characteristics at 90º stage rotation. In contrast, the feldspar is coarse with an indication of the grains being subjected to chemical weathering due to the rusting appearance of the grains. The feldspar and quartz composition plot in the Arkosic arenite (arkose) field on the ternary functional diagram of the rock classification. Similarly, the rock samples s26 and s32 plot on the arkose rock type region on the ternary functional diagram (Figure 4(a)). Sample s19 has 87% quartz and 13% feldspar with no indication of any rock fragments. The sample mineral composition plots on the sublithic arenite field on the ternary functional diagram for rock classification. Similarly, sample S29 comprises 77% Quartz composition, and 23% lithic with no indication of feldspar composition. The sample's mineral composition plot in the sublithic arenite field. However, sample s24 has fine to medium grains of quartz. The rock sample is poorly sorted. It comprises 96% quartz, and 4% feldspar with no lithic composition. The sample mineral composition is plotted in the quartz wacke field.

TABLE 1. The major oxide composition of the analyzed sedimentary sample

Sample ID	SiO_2 Wt %	TiO_2	Al_2O_3	Fe_2O_3	MnO	MgO	CaO	Na_2O	K_2O	P_2O_3
S10	76.7	0.99	17.5	1.19	0.0089	0.112	0.0881	0.0325	0.583	0.105
s20	78.4	0.945	15.2	1.05	BDL	0.138	0.0303	BDL	0.613	0.0609
s24	79.1	0.000157	18.4	3060	BDL	0.0203	0.0232	BDL	0.0744	0.1
s26	64.9	0.000163	31.5	1.6	BDL	0.0204	0.0211	BDL	0.084	0.133
s29	75.8	0.198	4.16	19.3	BDL	0.0328	0.0235	0.0231	0.0287	0.0672
s32	66	0.938	29.1	3.57	BDL	BDL	0.0289	BDL	0.0454	0.088
s33	71.4	0.000142	26.4	3300	BDL	0.0155	0.0209	BDL	0.0922	0.132
s34	58.3	0.000326	34.1	3.62	BDL	0.0243	0.0335	BDL	0.0804	0.168
s5	83.2	0.796	14.5	9460	BDL	0.0141	0.0097	BDL	0.0563	0.0446
s11	53.6	0.000256	42.2	6160	BDL	0.0217	0.022	BDL	0.0308	0.216
s14	54.1	0.000206	41.5	9430	BDL	0.0368	0.0809	BDL	0.058	0.145
s15	51.9	0.000216	39.1	2.16	BDL	0.072	0.063	BDL	0.339	0.172
s22	64.8	0.000206	26.5	1.19	102	0.174	0.0486	0.0237	0.894	0.102
s21	53.4	0.000136	30	5.65	BDL	0.514	0.0832	0.0301	0.00021	0.158
s23	435	0.000132	32.8	6.74	0.0102	0.505	0.116	0.0435	0.000197	0.391
s12	62.4	0.000175	28.8	2.66	BDL	0.326	0.0421	0.0385	BDL	0.134
Sum	1429	3.869115	431.76	51.871	0.0037	2.0269	0.735	0.1914	2.9796.08	2.2167
Minimum	51.9	0.000132	4.16	0.306	0.0089	0.0141	0.0097	0.0231	0.000197	0.0446
Maximum	435	0.99	42.5	19.3	0.0182	0.514	0.116	0.0435	0.8940	0.3910
Mean	89.31	0.24182	26.985	3.242	0.0124	0.1351	0.0459	0.01196	0.1986	0.1385
STD DEV.	92.76	0.407444	10.62	4.677	0.0051	0.1739	0.0310	0.0166	0.2772	0.0811

TABLE 2. The descriptive statistic of the Rare Earth elements composition in the analyzed samples

	N	Minimum	Maximum	Mean	Std. Deviation
La	18	14.334	313.154	193.11228	92.758727
Ce	18	43.653	2091.822	753.01022	587.172838
Pr	18	5.000	89.169	54.44872	26.350647
Nd	18	19.689	368.301	213.68583	107.576455
Sm	18	4.548	78.695	41.15400	22.466885
Eu	18	1.442	18.332	10.31472	5.876987
Gd	18	5.204	67.177	40.19367	20.598759
Tb	18	.771	8.402	4.59233	2.488695
Dy	18	4.046	40.701	20.20322	11.730632
Ho	18	.694	6.860	3.14456	1.960117
Er	18	1.721	17.933	7.74833	5.007407
Tm	18	.234	2.174	.93356	.608756
Yb	18	1.193	12.077	5.51594	3.299572
Lu	18	.279	1.851	.86200	.493770
Y	18	8.749	173.768	64.39544	41.945470
Valid N (listwise)	18				

TABLE 3. The Pearson correlation coefficient table indicating the validity of the major oxide data

	SiO_2	TiO_2	Al_2O_3	Fe_2O_3	MnO	MgO	CaO	Na_2O	K_2O	P_2O_3
SiO_2	1									
TiO_2	-.092	1								
Al_2O_3	.048	-.508*	1							
Fe_2O_3	-.147	-.003	.154	1						
MnO	.799**	-.007	.020	-.268	1					
MgO	.558*	-.220	.117	-.370	.528*	1				
CaO	.559*	-.118	.320	-.197	.675**	.694**	1			
Na_2O	.502*	-.094	-.164	-.441	.658**	.802**	.638**	1		
K_2O	-.160	.318	-.202	-.291	.337	-.052	.110	.076	1	
P_2O_3	.772**	-.490	.593*	-.118	.605*	.554*	.629**	.385	-.292	1

**. Correlation is significant at the 0.01 level (2-tailed)
*. Correlation is significant at the 0.05 level (2-tailed)

TABLE 4. The Pearson correlation coefficient table indicating the validity of the rare earth elements

	La	Ce	Pr	Nd	Sm	Eu	Gd	Tb	Dy	Ho	Er	Tm	Yb	Lu	Y
La	1														
Ce	.770**	1													
Pr	.971**	.705**	1												
Nd	.917**	.638**	.976**	1											
Sm	.839**	.570*	.927**	.969**	1										
Eu	.762**	.516*	.858**	.912**	.982**	1									
Gd	.733**	.520*	.819**	.850**	.937**	.970**	1								
Tb	.640**	.406	.739**	.772**	.883**	.936**	.982**	1							
Dy	.507*	.271	.614*	.645**	.772**	.841**	.915**	.973**	1						
Ho	.375	.171	.485	.510*	.627**	.690**	.795**	.879**	.960**	1					
Er	.323	.157	.431	.450	.542*	.584*	.699**	.782**	.884**	.977**	1				
Tm	.189	.085	.288	.304	.386	.426	.556*	.647**	.777**	.919**	.980**	1			
Yb	.147	.094	.226	.252	.333	.385	.513*	.584*	.699**	.838**	.906**	.946**	1		
Lu	.099	.073	.165	.186	.264	.315	.440	.519*	.647**	.804**	.883**	.937**	.991**	1	
Y	.054	-.041	.138	.177	.259	.310	.417	.509*	.649**	.809**	.885**	.936**	.971**	.982**	1

**. Correlation is significant at the 0.01 level (2-tailed)
*. Correlation is significant at the 0.05 level (2-tailed)

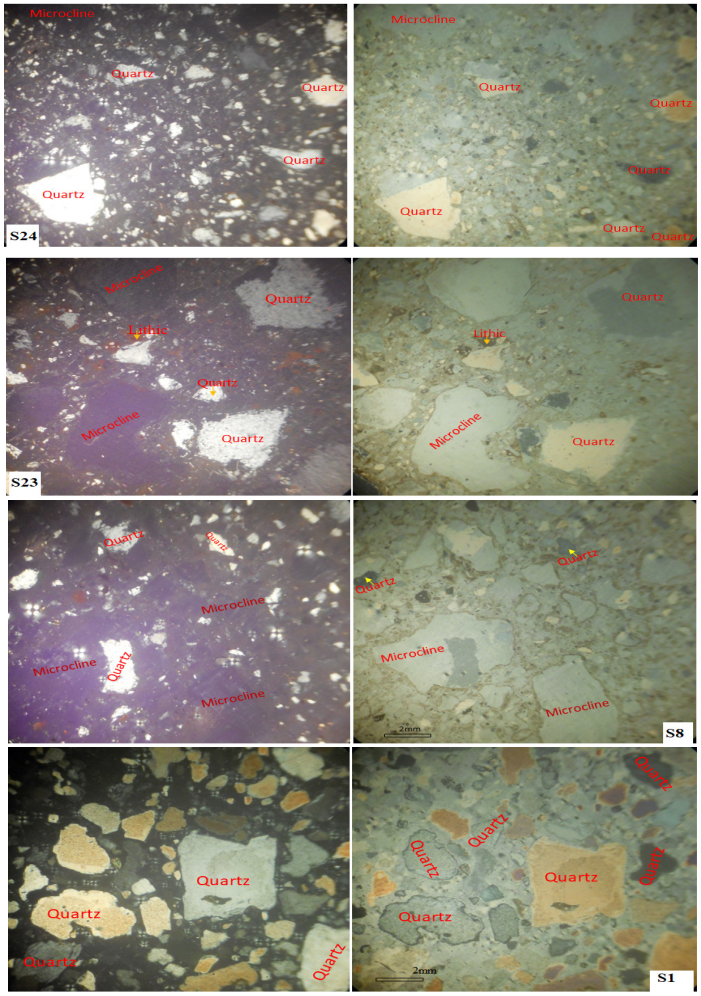

FIGURE 3. Photomicrograph showing the mineral composition of sandstone samples from the study area (XP is Crossed Polar; PP = Plane Polar; Q = Quartz; F=Feldspar and RF= Rock Fragment or Lithic)

TABLE 5. Modal composition of Quartz-Q, Feldspar-F and rock fragment-FR (Lithic) in the Lithofacies samples in the study area

Sample ID	Qt		F	Rf	M	C	% Composition			MMI	Lithofacies
	Qp	Qm					Q	F	RF		
S01	71	26	0	2	0.8	0.2	98	0	2	0.98	Quartz arenite
S8	50	15	35	0	0.4	0.6	65	35	0	0.65	Arkose
S11	18	5	76	0	0.2	0.8	23	77	0	0.23	Arkose
S19	67	19	0	13	0.6	0.4	87	0	13	0.87	Sublithic Arenite
S23	80	17	2	0	0.8	0.2	98	2	0	0.98	Quartz Arenite
S24	61	19	3	0	15.9	0.1	96	4	0	0.96	Quartz wacke
S26	60	11	28	0	0.3	0.7	72	28	0	0.72	arkose
S29	67	10	0	23	0.9	0.1	77	0	23	0.77	Sublithic arenite
S32	70	24	5	0	0.8	0.2	95	5	0	0.95	Arkose
S33	86	9	4	0	0.6	0.4	96	4	0	0.96	Quartz arenites

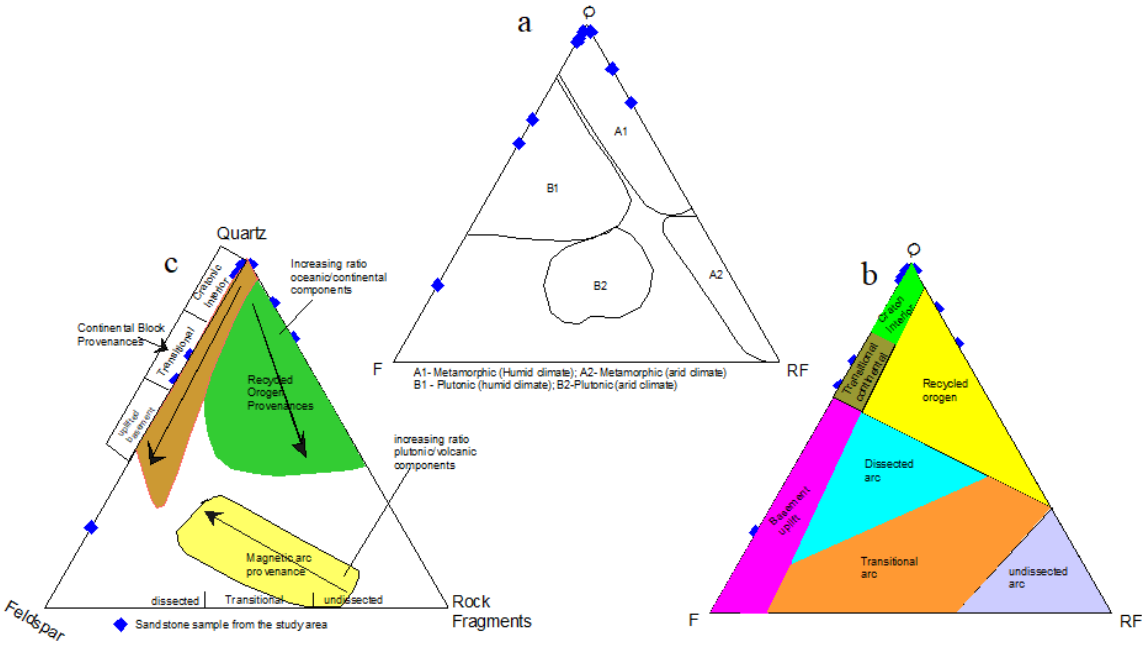

FIGURE 4. Triangular diagram of Quartz, Feldspar and Rock fragment composition in sandstone for Provenance and Palaeotectonic

PROVENANCE

Observation from the triangular variation diagram of Quartz=Q, Feldspar=F and Rock fragment=RF (Figure 4(c)) indicates a recycled orogeny provenance, interior cratonic and transitional (continental block) provenances. These indicate a metamorphic, igneous and sedimentary provenance (Figure 4(b) and 4(c)) with a humid climate. This is also supported by the enrichment of the light rare earth elements (LREE) and depleted heavy rare earth elements which indicate a felsic igneous provenance. The nature of the quartz grain's crystallinity (that is the polycrystalline and monocrystalline nature of the Quartz grain) is suggestive of more than a single source with the monocrystalline Quartz indicating a far source area from the sediment deposition area. However, the polycrystalline Quartz suggests an intra-basinal source, or an area close to or not too far from the sediment's deposition area. The presence of Arkosic arenite rock type in the study area also supports the intra-basinal provenance. The plutonic provenance is also supported by the microcline composition and the high refractive index of the Andesine a plagioclase series mineral observed under the petrographic microscope. The Andesine and microcline are mineralogical constituents of Diorite a plutonic rock (Mackenzie & Adams 2003; Nichols 2009). The sedimentary deposit in the study area was sourced from a plutonic and metamorphic origin. The metamorphic and the plutonic sources were part of the rifted plates. The cratonic interior, transitional continental, and uplifted basement (Figure 4(a) & 4(b)) later weathered due to the humid climate which favours rapid weathering. The weathered uplifted basement was deposited as a sedimentary rock which was later re-uplifted and weathered, transported, and deposited as the sediment in the study area, hence the recycled orogeny provenance (Figure 4(b) & 4(C)). Similarly, from the geochemistry perspective, a discriminant functional diagram was plotted based on Titanium, Aluminum, Iron, Calcium, Potassium, and Sodium oxides (after Roser & Korsch 1986) (Figure 5(a) & 5(b)). The sandstone samples plot on the Quartzose sedimentary provenance, intermediate igneous and Felsic igneous provenance which aligns with the observation from the petrographic approach. The normalized Rare Erath Element, REE (to the primitive mantle values) concentrations plotted on a vertical axis against the atomic number of the REEs indicated enrichment in cerium (Ce) and europium (Eu) concentrations (Figure 5(c)) which also confirms a felsic igneous provenance.

PALAEOTECTONIC

The tectonic indication from the plot of Quartz, Feldspar and Rock fragments on a triangular composition diagram (Figure 4(b) and 4(c)) shows the plotting of the sandstone samples in the cratonic interior, basement uplift, transitional continental crust and recycled orogeny field. These describe a Lithospheric (Continental Crust) Extension Tectonic which comprises rifting, subsidence and uplifting tectonic activities. The undulose extinction observed in

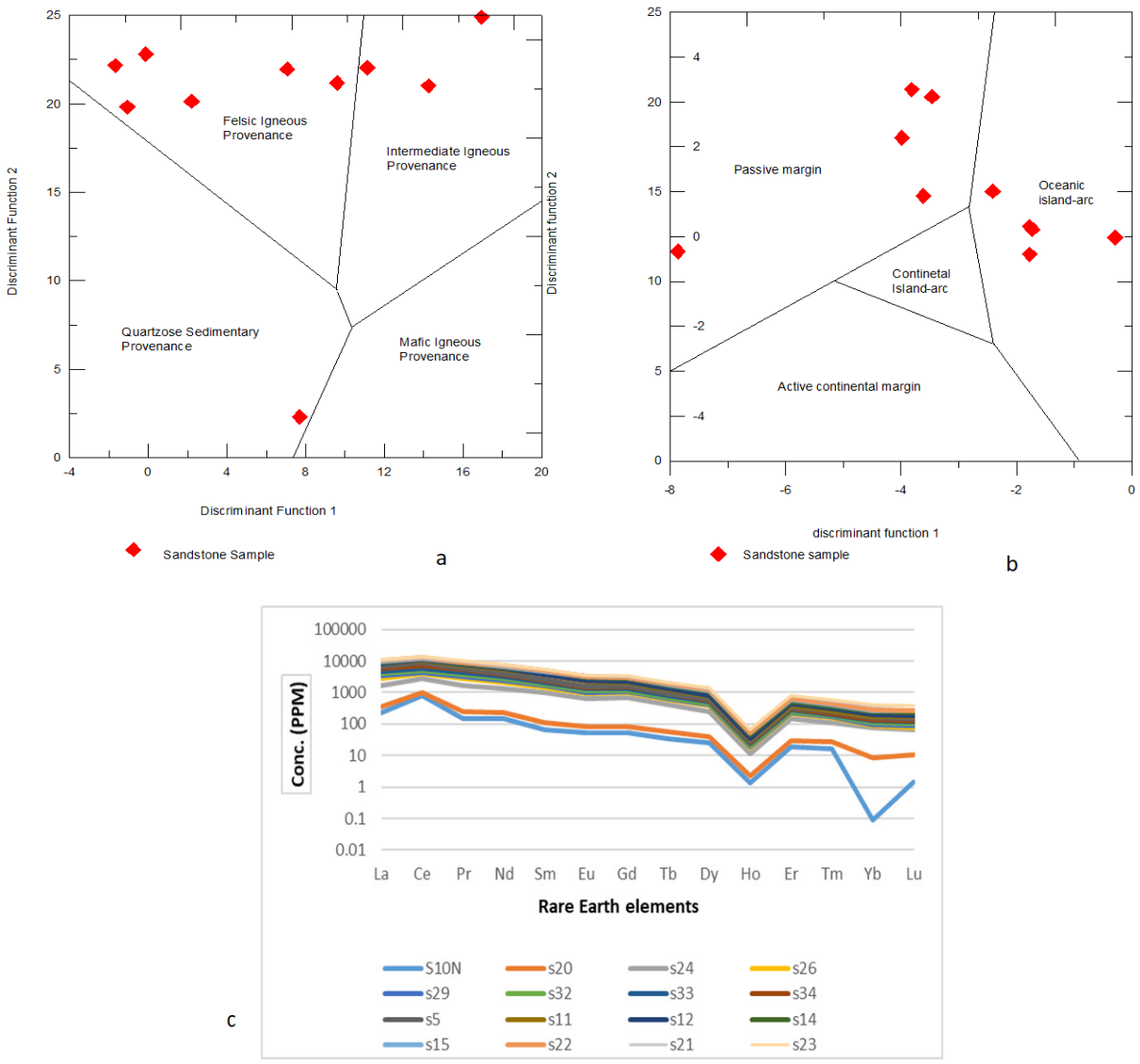

FIGURE 5. (a) Geochemical discrimination diagram for sandstone provenance using major element oxide (after Roser & Korsch 1986; Rollinson 1993). The sandstone samples plot in Felsic igneous, Quartzose sedimentary and intermediate igneous provenance fields, with Felsic igneous being the dominant field. Discriminant function 1 (Dft1) = -1.773TiO_2 + 0.607Al_2O_3 + 0.76Fe_2O_3 (total) - 1.5MgO + 0.616 CaO + 0.509Na_2O -1.224K_2O – 9.09. Discriminant function 2 (Dft1) = 0.445TiO_2 + 0.007Al_2O_3 – 0.25Fe_2O_3 (total) – 1.142MgO + 0.438CaO + 1.475Na_2O + 1.426K_2O – 6.861. (b) Palaeotectonic indication from the geochemistry of the sedimentary samples in the study area. Discriminant function 1 (Dfv1) =30.538TiO_2/Al_2O_3– 12.541Fe_2O_3 (total)/Al_2O_3 + 7.329MgO/Al_2O_3 + 12.031Na_2O/Al_2O_3 + 35.402K_2O/Al_2O_3 –6.382. Discriminant function 2 (Dfv2) = 50.500TiO_2/Al_2O_3 – 10.8795Fe_2O_3 (total)/Al_2O_3 + 30.875MgO/Al_2O_3 – 5.404Na_2O/Al_2O_3 + 11.112K_2O/Al_2O_3 – 3.89 (Table 4). (c) Rare earth elements concentrations of the sandstone samples normalised to primitive chondritic meteorite values (after Taylor & McLennan 1985)

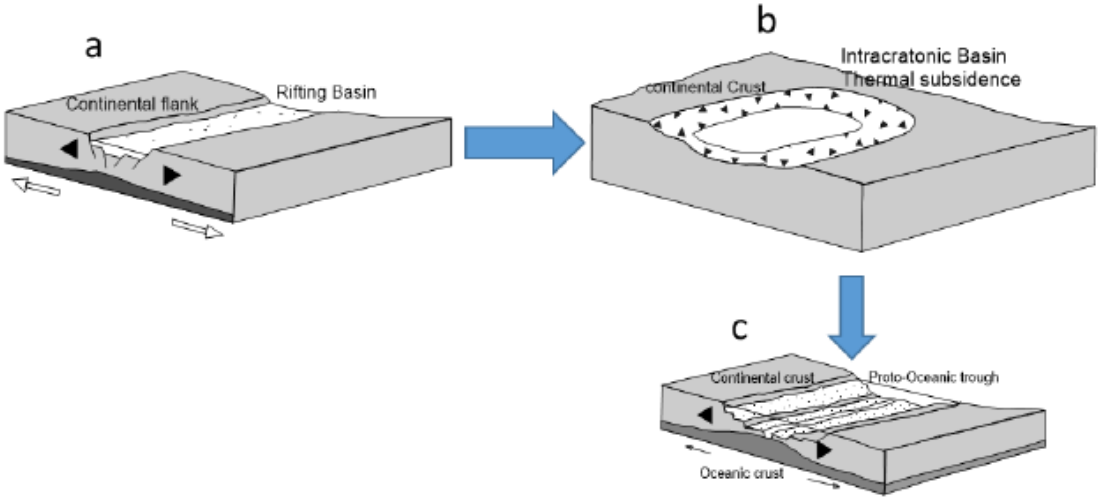

FIGURE 6. Model explaining the palaeotectonic evolution of the sedimentary deposit in the study area (modified after Nichols (2009) mechanism)

some of the Quartz grains of the studied sedimentary samples under the petrographic microscope also confirms the lithospheric extensional regime. Due to extensional stress, quartz from a lithospheric extension terrain exhibits an undulose extinction (Mackenzie & Adams 2003; Murakoshi & Masuda 1992; Nichols 2009). Similarly, the value of log (K_2O/Na_2O) was plotted against SiO_2 to infer the palaeotectonic from the geochemistry approach (after Bhatia 1983; Ogala et al. 2015; Ogbahon & Olujinmi 2019; Rollinson 1993; Roser & Korsch 1986). The samples were plotted on the passive margin (associated with divergent plate tectonic) and Oceanic island-arc (associated with convergent plates tectonic).

The tectonic pattern inferred from the petrographic approach also aligned with the palaeotectonic indication from the geochemistry of the sedimentary samples plotted on a geochemical functional diagram for palaeotectonic in Figure 5(b). Passive margin is associated with continental crust rifting and is affected by thermal, isostatic, and mantle stresses (Nichols 2009). Based on the tectonic indication from both petrographic and geochemistry approaches, the mechanism of the palaeotectonic evolution of the sedimentary deposit in the study area can be explained as follows.

The heat energy from a thermal plume in the Mantle led to an increase in the heat energy flow within the crust situated over the thermal plume. This subjected the crust to intense stress which resulted in the rupturing of the continental crust breaking into three branches (Figure 6). These three branches are known as the Triple Junction or arms along which the lithospheric extension occurs. This describes the lithospheric extension tectonic regime. This regime has three developmental stages: The continental rift stage, the proton-ocean trough stage and the young ocean basin (similar to the three developmental periods explained by Murakoshi & Masuda 1992; Nichols 2009). The continental crust built up extensional stress at the continental rift stage due to the lithospheric plate's movement. The continental crust then fractured to create RIFTS, a structural valley of an extensional fault formed due to horizontal extensional stress (this is confirmed by the undulose extinction observed in some of the Quartz grains). The uplifted continental crust on the rifted flanks formed a sediment source for the rift valley. The continental crust in the third arm of the triple junction was formed and extended at the continental rift stage. Rifting ceased at this stage and the continental crust at the rift area began to cool, contract and sink to form a subsidence known as a failed arm or failed rift (Figure 6(b), (similar to the Intracratonic basin observed by Nichols (2009). This basin received fluvial and lacustrine deposits which were later uplifted, weathered, transported, and deposited as part of the sediments in the study area. However, the lithospheric extension continues in the other two arms until the proto-ocean trough stage and young ocean basin stage are formed (Figure 6(c)). At this stage, the continental crust in the first two arms of the triple junction rifted completely to form a new ocean. The plot of some samples on the Oceanic Island arc suggests the study area received some sediment produced from convergent tectonic plates associated with the oceanic crust.

CONCLUSION

The siliciclastic deposits of the Mamu Formation around Imiegba in southern Nigeria are traced to an igneous, metamorphic, and sedimentary origin with a combined input of divergence and convergence tectonic activities. The divergence tectonic was dominant and comprised activities including a continental crust extension, rifting, subsidence, and uplifting and weathering of the uplifted continental crust. The weathered sediment was transported and deposited on a passive margin. However, the convergent tectonic consists of lithospheric collision, subduction and frictional destruction of the crust and weathering of the oceanic island arc. The weathered sediment produced from convergence tectonic was transported and deposited as part of the sediment in the study area through transgression. The use of subsurface samples is recommended for future research in the study area to further investigate and substantiate the findings of the current research.

ACKNOWLEDGEMENTS

The first author is grateful to the American Association of Petroleum Geologists (AAPG), who have contributed to his educational program over the years and this research work, respectively. Your assistance and contributions have made this research work possible and successful.

REFERENCES

Adeigbe, O.C. & Salufu, A.E. 2009. Geology and depositional environment of Campano-Maastrichtian sediments in the Anambra Basin, Southeastern Nigeria: Evidence from field relationship and sedimentological study. *Earth Sciences Research Journal* 13(2): 58-75.

Ameh, E.G. 2019. Geochemistry and multivariate statistical evaluation of major oxides, trace and rare earth elements in coal occurrences and deposits around Kogi East, Northern Anambra Basin, Nigeria. *International Journal of Coal Science and Technology* 6(2): 260-273.

Bhatia,.M.R. 1983. Plate tectonics and geochemical composition of sandstones. *Journal of Geology* 91: 611-627.

Edegbai, A.J., Schwark, L. & Oboh-Ikuenobe, F.E. 2020. Nature of dispersed organic matter and paleoxygenation of the Campano-Maastrichtian dark mudstone unit, Benin flank, western Anambra Basin: Implications for Maastrichtian Trans-Saharan seaway paleoceanographic conditions. *Journal of African Earth Sciences* 162: 103654.

James, E., Ghani, A.A., Akinola, O.O. & Asis, J. 2021. Petrology and geochemical features of Semporna volcanic rocks, South-East Sabah, Malaysia. *Sains Malaysiana* 50(1): 9-21.

Körmös, S., Bechtel, A., Sachsenhofer, R.F., Radovics, B.G., Milota, K. & Schubert, F. 2020. Petrographic and organic geochemical study of the Eocene Kosd Formation (northern Pannonian Basin): Implications for paleoenvironment and hydrocarbon source potential. *International Journal of Coal Geology* 228: 103555.

Mackenzie, W.S. & Adams, A.E. 2003. *A Colour Atlas of Rock and Minerals in Tin Section.* Seventh: Manson Publishing Ltd.

Madukwe, H. & Obasi, R. 2015. Classification, maturity, provenance, tectonic setting and source-area weathering of the Ilubirin stream sediments, South West, Nigeria. *International Journal of Sciences* 1(04): 7-21.

Murakoshi, N. & Masuda, F. 1992. Estuarine, barrier-island to strand-plain sequence and related ravinement surface developed during the last interglacial in the Paleo-Tokyo Bay, Japan. *Sedimentary Geology* 80(3-4): 167-184.

Nichols, G. 2009. *Sedimentology and Stratigraphy*. 2nd ed. Chichester: John Wiley & Sons Ltd.

Nigerian Geological Survey Agency (NGSA). 2006. *Geological and Mineral Resources Map of Edo State*.

Nwanjide, C.S. 2013. *Geology of Nigeria's Sedimentary Basins*. Lagos: CSS Bookshops Ltd.

Obaje, S.O. 2019. Granulometric and geochemical assessment of ajali sandstone in fugar area in benin flank of Anambra Basin, Nigeria. *FULafia Journal of Science and Technology* 5(2): 78-87.

Ogala, J.E., Olobaniyi, S.B., Omo-Irabor, O.O. & Adaikpoh, E.O. 2015. Petrographic and geochemical study of the Maastrichtian Ajali Sandstone, North Central Nigeria. *Geological Quarterly* 59(1): 79-90.

Ogbahon, O.A. & Olujinmi, O.B. 2019. Geochemistry of Maastrichtian clastic sedimentary rocks from western flank of Anambra Basin, Nigeria: Implications for provenance, tectonic setting, paleoclimate and depositional paleoenvironment. *International Journal of Geosciences* 10(01): 91-118.

Okoro, A., Igwe, E. & Nwajide, C. 2016. Sedimentary and petrofacies analyses of the Amasiri sandstone, southern Benue Trough, Nigeria: Implications for depositional environment and tectonic provenance. *Journal of African Earth Sciences* 123: 258-271.

Overare, B., Osokpor, J., Ekeh, P.C. & Azmy, K. 2020. Demystifying provenance signatures and paleo-depositional environment of mudrocks in parts of south-eastern Nigeria: Constraints from geochemistry. *Journal of African Earth Sciences* 172: 103954.

Pettijohn, F.J., Potter, P.E. & Siever, R. 1987. *Sand and Sandstone.* New York: Springer.

Rollinson, H. 1993. *Using Geochemical Data: Evaluation, Presentation, Interpretation.* England: Longman.

Roser, B.P. & Korsch, R.J. 1986. Determination of tectonic setting of sandstone-mudstone suites using SiO_2 content and K_2O/Na_2O ratio. *The Journal of Geology* 94(5): 635-650.

Taylor, S.R. & McLennan, S.M. 1985. *The Continental Crust: Its Composition and Evolution*. Melbourne: Blackwell Scientific.

Tijani, M.N., Nton, M.E. & Kitagawa, R. 2010. Textural and geochemical characteristics of the Ajali Sandstone, Anambra Basin, SE Nigeria: Implication for its provenance. *Comptes Rendus - Geoscience* 342(2): 136-150.

*Corresponding author; email: bib@ukm.edu.my

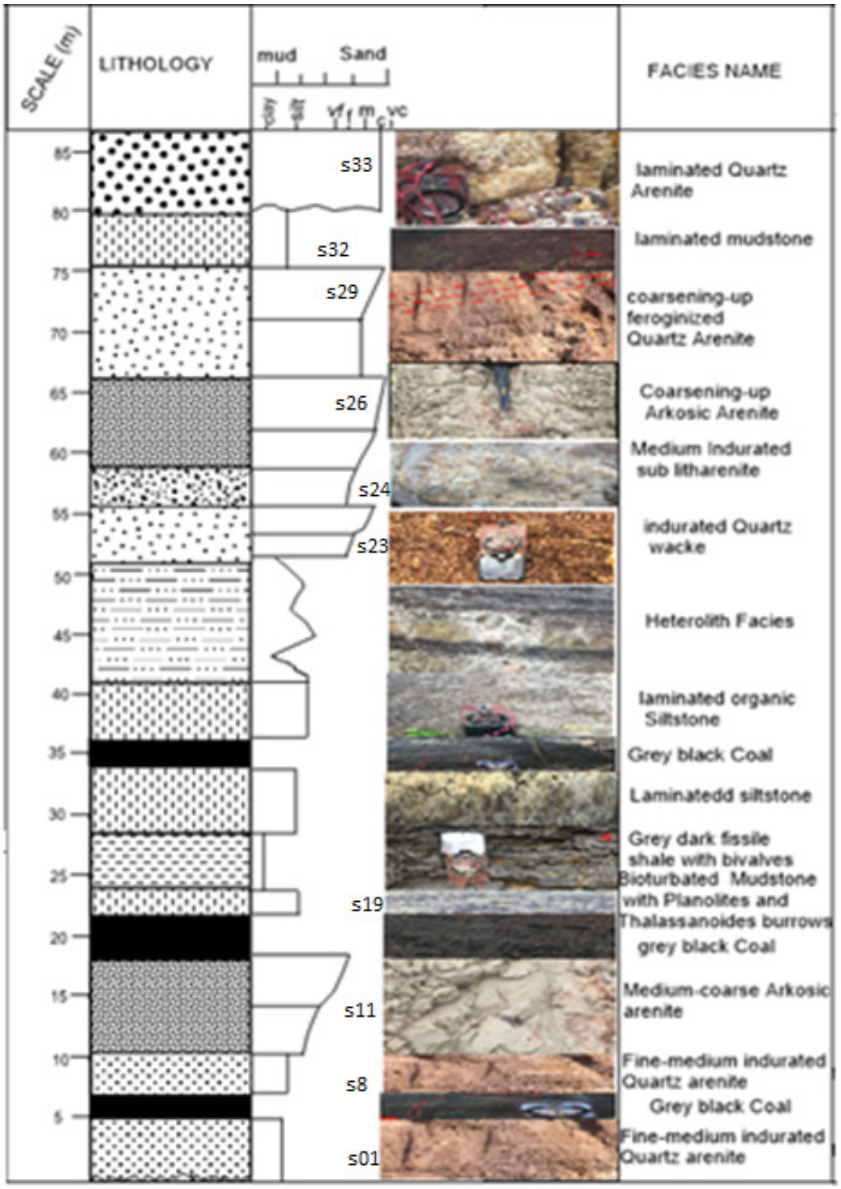

SUPPLEMENTARY 1. Lithofacies description of the study area

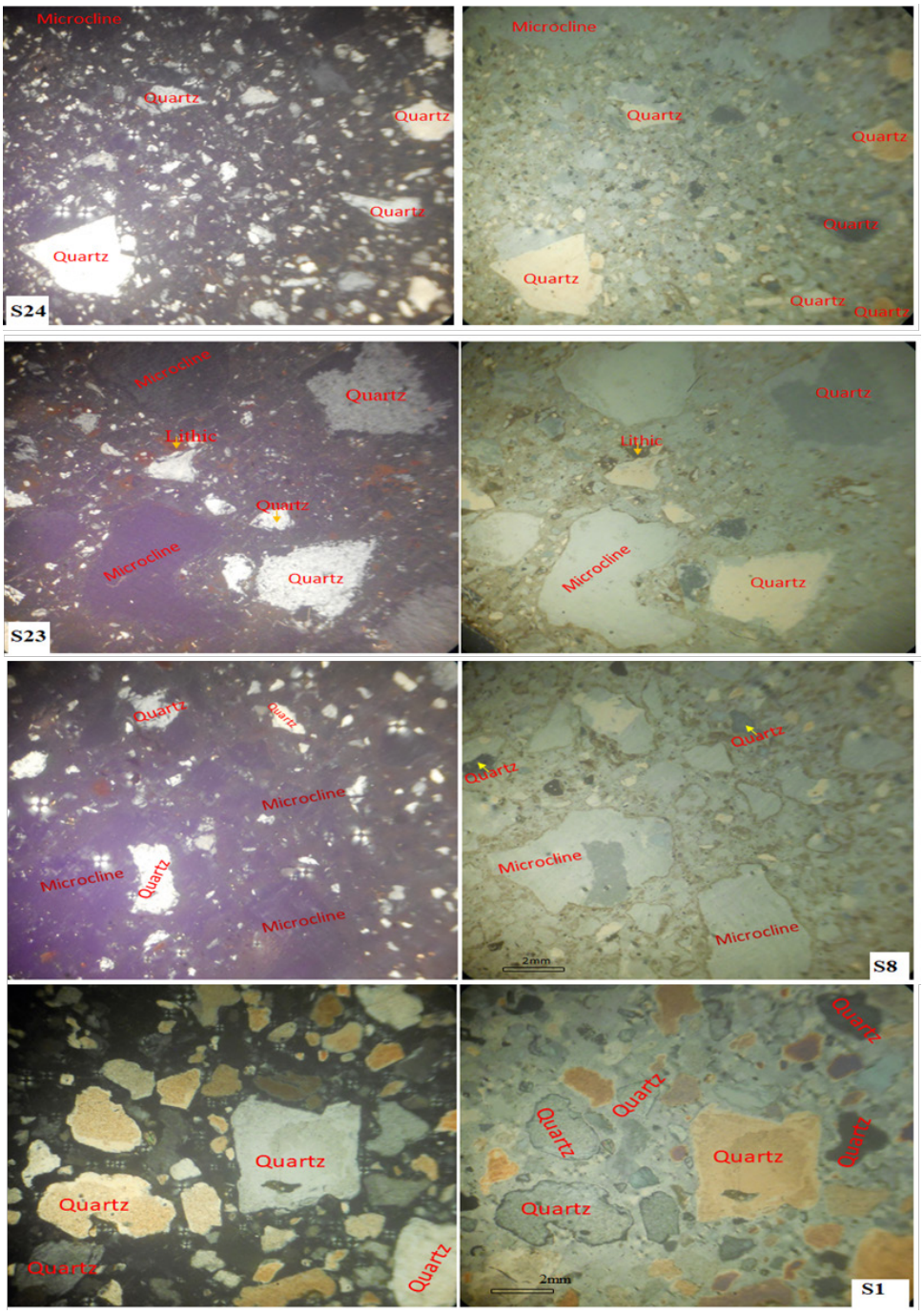

SUPPLEMENTARY 2. Photomicrographs of the sandstone samples from the study area. P=Plagioclase; M=Microcline; F=Feldspar; Q=Quartz; RF= rock fragment

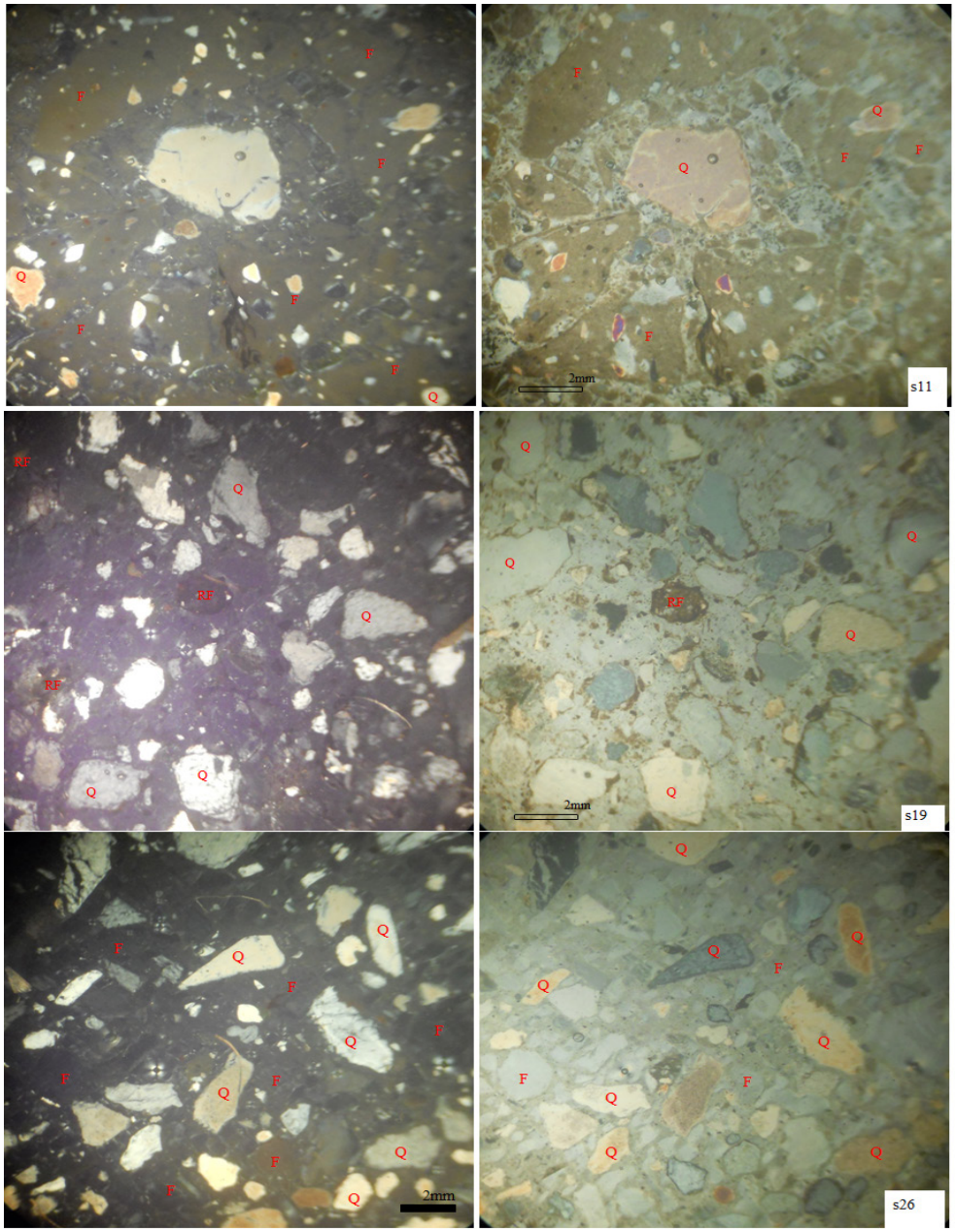

SUPPLEMENTARY 3. Photomicrographs of the sandstone samples from the study area. P=Plagioclase; M=Microcline; F=Feldspar; Q=Quartz; RF= rock fragment

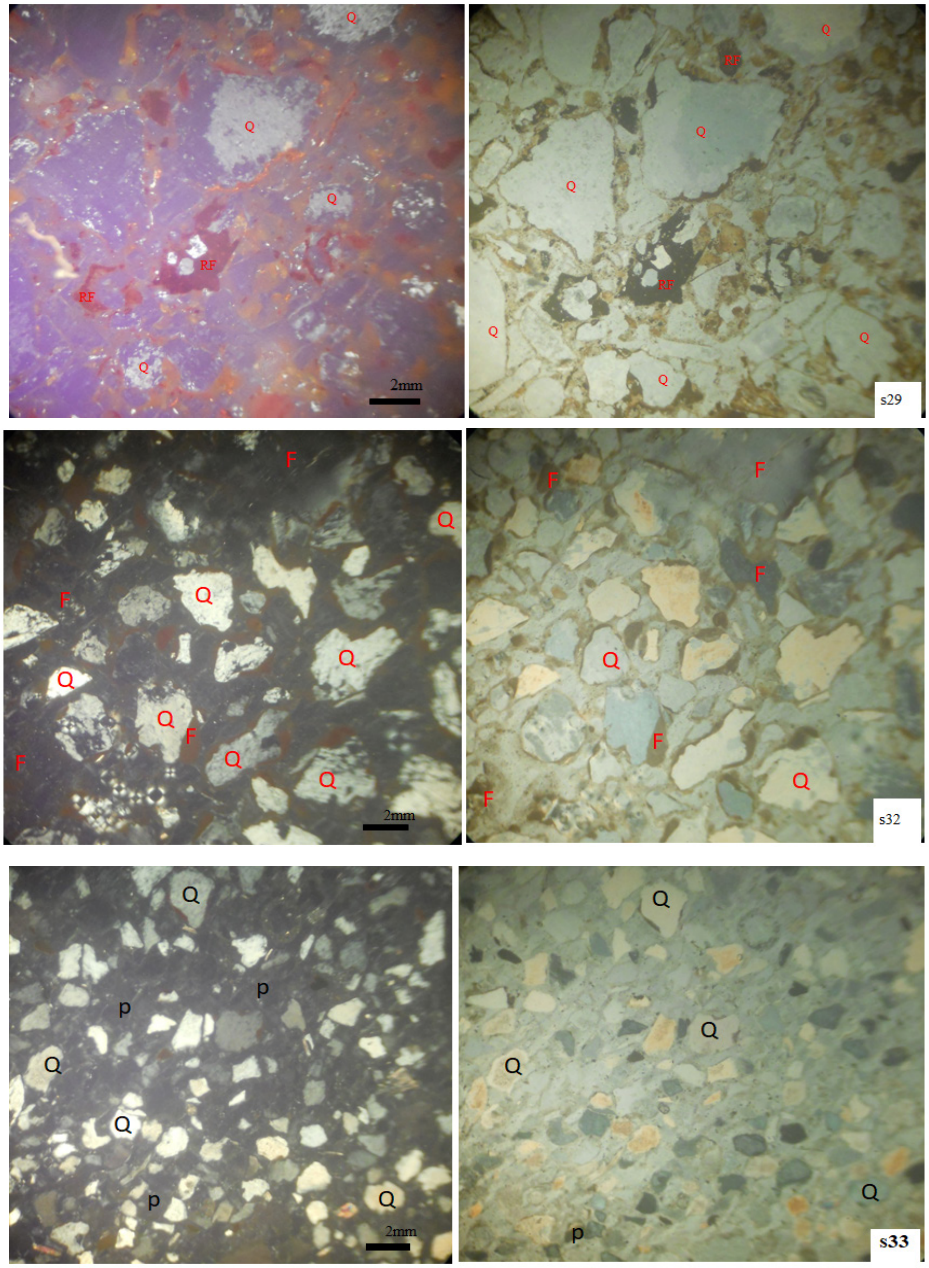

SUPPLEMENTARY 4. Photomicrographs of the sandstone samples from the study area. P=Plagioclase; M=Microcline; F=Feldspar; Q=Quartz; RF= rock fragment